Long-Distance Free-Space Distribution of Quantum Entanglement

Markus Aspelmeyer, *et al.*

Long-Distance Free-Space Distribution of Quantum Entanglement

Markus Aspelmeyer,* Hannes R. Böhm, Tsewang Gyatso, Thomas Jennewein, Rainer Kaltenbaek, Michael Lindenthal, Gabriel Molina-Terriza, Andreas Poppe, Kevin Resch, Michael Taraba, Rupert Ursin, Philip Walther, Anton Zeilinger†
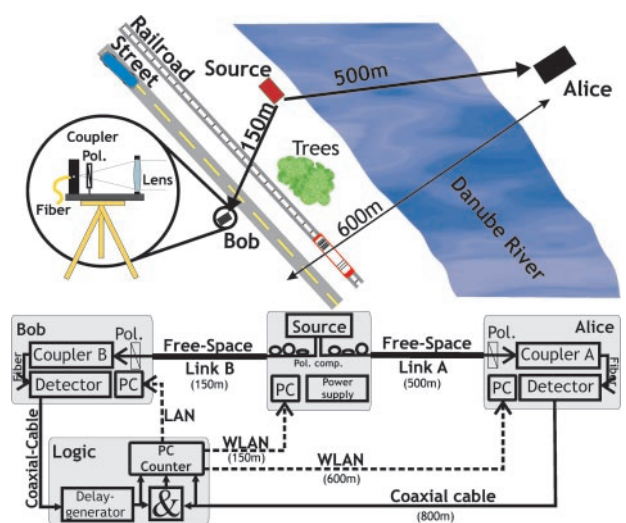
We demonstrate the distribution of quantum entanglement via optical free-space links to independent receivers separated by 600 m, with no line of sight between each other. A Bell inequality between those receivers is violated by more than four standard deviations, confirming the quality of the entanglement. This outdoor experiment represents a step toward satellite-based distributed quantum entanglement.

Quantum entanglement is a fundamental feature of quantum mechanics and is central to most advanced quantum communication applications (*1*, *2*). At present, most realizations of quantum communication schemes are based on entangled photon pairs, which are shared over long distances with the use of optical-fiber links. In these experiments, entanglement has been distributed over distances ranging from several hundred meters up to 10 km (*3–5*). In all cases, violation of a Bell inequality was used as the experimental measure for proving that entanglement was indeed shared between the separate observers. On the basis of present fiber and detector technology, it has been determined that absorptive losses limit the distances over which entanglement can be shared to the order of 100 km (*6*, *7*). Without the addition of (as-yet undemonstrated) quantum repeaters (*8*), the extent over which one can quantum communicate is restricted to this distance over which entanglement can be distributed. Free-space optical links provide a way to overcome these limitations. Earth-based free-space links are also limited in distance due to obstructing objects in the line of sight, atmospheric attenuation because of weather conditions and aerosols (*9*) and, ultimately, the curvature of Earth. The use of satellite technology will permit those distances to be bridged beyond the capability of Earth-based stations, eventually leading to a truly global distribution of entangled photons and thus to novel possibil-

ities for fundamental quantum physics research and quantum communication applications. Recently, several groups have succeeded in distributing faint classical laser pulses via free-space links over distances up to several kilometers to demonstrate free-space quantum cryptography (*10*, *11*, *12*). We have taken the next step and demonstrated the free-space distribution of entangled photons over long distances between two independent receiver stations.

In our setup, the two receivers were located at different sides of the Danube River in Vienna, Austria, on the rooftops of two build-
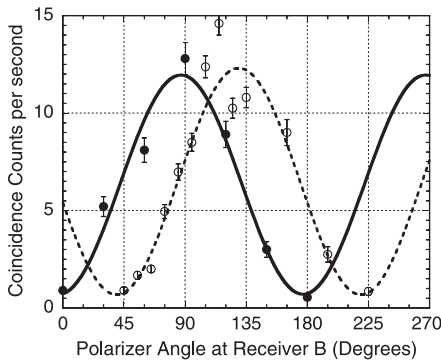
ings approximately 600 m apart. The actual measurements took place during night at outside temperatures around 0° C and wind strengths up to 50 km/h, thereby demonstrating the robustness of our source and links against less than ideal environmental conditions. The receiver stations were located at distances of 150 and 500 m, respectively, from the entangled photon source and did not have a direct line of sight to one another due to obstruction from trees and power lines (Fig. 1).

Each photon from the entangled pair emitted by the source was coupled into a single-mode optical fiber. The fibers were connected to independent sending telescopes that consisted of a single-mode fiber coupler located approximately in the focal plane of a 5-cm-diameter lens. Each receiver terminal was equipped with a similar telescope (with the addition of a polarizer), which was aligned to couple the incoming entangled photons back into single-mode fibers for detection in single-photon–counting avalanche photo diodes with a detection efficiency of about 40%. Due to the spatial selectivity of the single-mode fibers (*13*), no bandpass filters were required at the source or at the receivers to discriminate the signal from the background light during night operation. However, the end of a measurement run was sharply marked by the onset of sunrise, which increased the background from almost zero to several thousands per second in only a few minutes.

Fig. 1. Bird's-eye view and block diagram of the experiment. Compared with the standard laboratory environment, the less-than-ideal experimental conditions include close to 0°C temperatures and strong wind gusts at all stations, as well as passing freight trains and trucks affecting the link B and passing ships on the Danube close to the link A. The line of sight between the receiver stations A and B (Alice and Bob) was obstructed mainly by trees. The inset shows the schematics of a receiving telescope, which includes the analyzing polarizer. All telescopes were mounted on tripods and thus were affected by wind gusts, which induced signal scintillation at the receiver stations. This effect was drastically reduced by the use of plastic boxes (actually compost bins), which served as protective windshields. The time delay between the arrival times of the pulses of a pair at receiver B was adjusted by an electronic delay generator. Instead of separate counting devices, Wave-LAN (WLAN) connections were established between a central counting unit (also housing the coincidence logic and delay generator) and several laptop computers at the telescope stations and the source. This allowed access to singles and coincidence count rates from all stations for alignment purposes and data acquisition.

Institut für Experimentalphysik, Universität Wien, Boltzmanngasse 5, A-1090 Wien, Austria.

*To whom correspondence should be addressed. E-mail: markus.aspelmeyer@quantum.at or zeilinger-office@quantum.at
†All authors contributed equally to this work.

As a source for polarization-entangled photons, we used type II spontaneous parametric down-conversion (SPDC) (*14*), pumped by a violet laser diode operating at 405 nm to produce nearly energy degenerate pairs at 810 nm. With a pump power of 18 mW, we measured ~120,000 s^{-1} single photons in each arm of the source and approximately 20,000 polarization entangled photon pairs per s, which were coupled into single-mode fibers to the telescopes. Visibilities of the polarization correlations, which indicate the quality of the entanglement, were found to be larger than 97% in the 0°/90° basis and larger than 94% in the 45°/135° basis, before coupling them to the long-distance free-space telescope links. The setup for the source has been miniaturized to fit on a small optical breadboard, and it could easily be transported from the laboratory to the outdoor field site, where it was kept in a small shielded container. Electrical power for the source was provided by a gasoline-driven power generator, which makes it completely independent from an ideal laboratory environment.

The attenuation in each of the links was about 12 dB (6% transmission) without taking into account the efficiency of the detectors (*15*). In total, local single count rates of ~4000 s^{-1} (including background) and a maximum coincidence rate of 15 s^{-1} could be observed. The local singles background rates were 650 s^{-1} and 750 s^{-1} at receivers A and B, respectively. The background was almost entirely due to the dark count rates of the detectors, while other background was highly suppressed by the spatial selectivity of

the single-mode fibers and by the nighttime operation (*16*).

Our SPDC source was aligned to produce the singlet state

$$|\Psi^-\rangle = \frac{1}{\sqrt{2}}\left(|H\rangle_A|V\rangle_B - |V\rangle_A|H\rangle_B\right),$$

which is one of the four maximally entangled Bell states. H and V denote horizontal and vertical polarization, respectively, and A and B indicate the different spatial modes in which the photons are collected. To show the quality of the distributed entanglement between the separate observers, we measured a series of polarization correlations that was eventually used to show a violation of a Bell inequality. The polarization correlation coefficients are given by

$$E(\phi_A,\phi_B) = \frac{N^{++} + N^{--} - N^{+-} - N^{-+}}{N^{++} + N^{--} + N^{+-} + N^{-+}}, \quad (1)$$

where N is the number of coincident detection events between the observers when the polarizers are set to ϕ_A (denoted by "+") or the corresponding orthogonal $\phi_A^\perp$ (denoted by "−") at receiver A and ϕ_B (denoted by "+") or $\phi_B^\perp$ (denoted by "−") at receiver B. In general, the coincidence count rate is given by $N(\phi_A,\phi_B) = 1/2 \sin^2(\phi_A - \phi_B)$. The experimental data exhibit this behavior (Fig. 2). The quality of the state ρ observed at the receiver stations can be defined by the fidelity $F = \langle\Psi^-|\rho|\Psi^-\rangle$. The correlation coefficient can be calculated from $F = [3E(\phi,\phi)+1]/4$, where $E(\phi,\phi)$ is the two-photon visibility for orthogonal polarization. With a visibility of 0.81 ± 0.02 in the H/V-basis and 0.85±0.02 in the 45°/135° basis, we obtain an average fidelity of (87 ± 3)%, which clearly overcomes the critical limit of 78% necessary to violate a Bell inequality (*17*). This fidelity was preserved over more than 2 hours, indicating the stability of the source and the links at the field site.

Further correlation coefficients were measured for a test of the Clauser-Horne-Shimony-Holt (CHSH) inequality (*18*), which, in contrast to the original Bell inequality (*19*), allows for nonperfect corre-

lations by introducing experimentally accessible expectation values $E(\phi_1,\phi_2)$. We used single-output analyzers, i.e., a polarizer, instead of two-output analyzers such as a polarizing beamsplitter. The CHSH-inequality has the form

$$S = |E(\phi_A,\phi_B) - E(\phi_A,\tilde{\phi}_B) + E(\tilde{\phi}_A,\phi_B) + E(\tilde{\phi}_A,\tilde{\phi}_B)| \leq 2\tilde{\phi}, \quad (2)$$

where S is the "Bell parameter." The quantum-mechanical prediction for photon pairs in the singlet state is $E(\phi_A,\phi_B) = -\cos[2(\phi_A - \phi_B)]$. The value for S is maximized for the set of angles $\{\phi_A,\tilde{\phi}_A,\phi_B,\tilde{\phi}_B\} = \{0°,45°,22.5°,67.5°\}$ to $2\sqrt{2} \approx 2.828$, which violates the limit of 2 and thus leads to a contradiction between local realistic theories and quantum mechanics. The experimentally obtained correlation coefficients are shown in Table 1. Using those values, we find $S = 2.41 \pm 0.10$, demonstrating the violation of a Bell inequality by 4.1 standard deviations. Due to the low background level, no additional data correction was necessary. These results clearly demonstrate that the two separated receiver stations share an entangled quantum state distributed to them via free-space optical links.

One of the benefits of a free-space distribution of quantum entanglement is the possibility of bridging large distances by additional use of space infrastructure such as satellites. Free-space links will provide a unique means to study fundamental limits due to long-distance deterioration of quantum correlations because of decoherence. In contrast, free-space quantum channels may provide the means to build truly global quantum communication networks. In the specific example of quantum cryptography, quantum entanglement enables secure key generation between the parties sharing entanglement (*20*), whereas the violation of a Bell inequality can provide a security test of the protocol (*21*). Although we did not intend to establish a cryptographic protocol, we can estimate the results for a cryptographic scheme based on entangled photons (*22, 23*). A raw key is established by the anti-correlated detection events, which are obtained when both receivers randomly choose the same basis. A cryptographic system based on our setup would have shown a total raw key generation rate of a few tens of bits per second and an estimated quantum bit error rate (QBER) of ~8.4%. We believe that these numbers can be improved significantly through improvements in telescope design.

Our link attenuation of 12 dB corresponds to a value that might be achievable with state-of-the-art space technology when establishing a free-space optical link between an Earth-based receiver telescope of 100 cm diameter and a satellite-based transmitter telescope of 20 cm diameter orbiting earth at a distance of ~600 km (*24*). Typical losses in an actual satellite

Fig. 2. Measured polarization correlations between receivers. The data show the measured coincidence rate (per second) between the two receivers as a function of the angle of the polarizer at receiver B when the polarizer at receiver A was set to 0° (solid circles, solid line) and to 45° (open circles, dotted line) respectively. The obviously noisy part in the data coincides with the passing of a freight train underneath the link to receiver B. Amplitude, offset, and phase were varied for the fitting routine, resulting in a phase offset from the theoretical prediction of (3.0 ± 1.5)° for the solid line and (5.4 ± 0.9)° for the dotted line. The visibilities of the best fit curves are (88.2 ± 5.7)% and (89.0 ± 3.3)%.

Table 1. Experimentally determined correlation coefficients to test for the violation of a Bell inequality. The integration time for each of the 16 data points (4 for every E) was 20 s, and each data point was averaged over at least two subsequent measurements (typically three). To take into account environmentally induced scintillation of our signal, we conservatively estimated the error as standard deviation of the count rate distribution.

(ϕ_A,ϕ_B)	$E(\phi_A,\phi_B)$
(0°,22.5°)	−0.509 ± 0.057
(0°,67.5°)	+0.643 ± 0.042
(45°,22.5°)	−0.558 ± 0.055
(45°,67.5°)	−0.702 ± 0.046

experiment might vary, depending on the link optics and on the performance of satellite pointing and tracking (*25*, *26*). Even then, our results represent an encouraging basis for future space experiments with entangled photons.

References and Notes

1. E. Schrödinger, *Naturwissenschaften* **23**, 807 (1935).
2. D. Bouwmeester, A. Ekert, A. Zeilinger, Eds., *The Physics of Quantum Information* (Springer-Verlag, Berlin, 2000).
3. P. R. Tapster, J. G. Rarity, P. C. M. Owens, *Phys. Rev. Lett.* **73**, 1923 (1994).
4. W. Tittel, J. Brendel, H. Zbinden, N. Gisin, *Phys. Rev. Lett.* **81**, 3563 (1998).
5. G. Weihs, T. Jennewein, C. Simon, H. Weinfurter, A. Zeilinger, *Phys. Rev. Lett.* **81**, 5039 (1998).
6. E. Waks, A. Zeevi, Y. Yamamoto, *Phys. Rev. A* **65**, 52310 (2002).
7. N. Gisin, G. Ribordy, W. Tittel, H. Zbinden, *Rev. Mod. Phys.* **74**, 145 (2002).
8. H.-J. Briegel, W. Dür, J. I. Cirac, P. Zoller, *Phys. Rev. Lett.* **81**, 5932 (1998).
9. H. Horvath *et al.*, *J. Geophys. Res.* **107**, 4386 (2002).
10. W. T. Buttler *et al.*, *Phys. Rev. Lett.* **81**, 3283 (1998).
11. R. J. Hughes, J. E. Nordholt, D. Derkacs, C. G. Peterson, *New J. Phys.* **4**, 43 (2002).
12. C. Kurtsiefer *et al.*, *Nature* **419**, 450 (2002).
13. C. Kurtsiefer, M. Oberparleiter, H. Weinfurter, *Phys. Rev. A* **64**, 23802 (2001).
14. P. G. Kwiat *et al.*, *Phys. Rev. Lett.* **75**, 4337 (1995).
15. The low coupling efficiency is mainly due to large beam diameters and high beam divergence because of small telescope lenses. A more sophisticated design of coupling telescopes can certainly achieve the diffraction-limited optimum.
16. Materials and Methods are available as supporting material on *Science* Online.
17. Correlation measurements were performed independently from the sine-curve measurements (Fig. 2).
18. J. F. Clauser, M. A. Horne, A. Shimony, R. A. Holt, *Phys. Rev. Lett.* **23**, 880 (1969).
19. J. Bell, *Physics* **1**, 195 (1964).
20. A. K. Ekert, *Phys. Rev. Lett.* **67**, 661 (1991).
21. C. Fuchs, N. Gisin, R. B. Griffiths, C. S. Niu, A. Peres, *Phys. Rev. A* **56**, 1163 (1997).
22. C. H. Bennett, G. Brassard, N. D. Mermin, *Phys. Rev. Lett.* **68**, 557 (1992).
23. T. Jennewein, C. Simon, G. Weihs, H. Weinfurter, A. Zeilinger, *Phys. Rev. Lett.* **84**, 4729 (2000).
24. M. Aspelmeyer *et al.*, "Quantum communications in space," *Tech. Rep. under contract 16358/02*, European Space Agency, in press.
25. J. E. Nordholt, R. Hughes, G. L. Morgan, C. G. Peterson, C. C. Wipf, *Proc. SPIE*, **4635**, 116 (2002).
26. J. G. Rarity, P. R. Tapster, P. M. Gorman, P. Knight, *New J. Phys.* **4**, 82 (2002).
27. This work was supported by the Austrian Science Foundation (FWF), Sonderforschungsbereich (SFB) 015 "Control and Measurement of Coherent Quantum Systems," the European Commission, Project IST-1999-10033 "Long Distance Photonic Quantum Communication" and by the companies Wien Kanal Abwassertechnologien Ges.m.b.H., Energie AG Oberösterreich, T-systems Austria GmbH (Network Services) and by the City of Vienna. Further funding for team members was provided by the FWF (G.M.-T.), the Austrian Exchange Service OAD (T.G.), ARC Seibersdorf research GmbH (H.R.B., A.P.), the Natural Sciences and Engineering Research Council of Canada (K.R.), and the Alexander von Humboldt Foundation (M.A.).

Surface-Driven Switching of Liquid Crystals Using Redox-Active Groups on Electrodes

Yan-Yeung Luk and Nicholas L. Abbott*

Electrochemical control of the oxidation state of ferrocene-decorated electrodes leads to surface-driven changes in the orientations of thermotropic liquid crystals. When the electrodes possess nanometer-scale topography, voltages of 0.0 to 0.3 volts (versus a counter electrode in a two-electrode cell) can drive changes in the orientation of the liquid crystals in the plane and/or out of the plane of the electrodes. Electrodes not supporting ferrocene do not lead to surface-driven orientational transitions. The in-plane transitions are driven by the reorganization of the monolayer of ferrocene upon oxidation of ferrocene to ferrocenium. The out-of-plane transition reflects a dielectric coupling between the liquid crystal and the diffuse part of an electrical double layer that evolves upon oxidation of ferrocene to ferrocenium. These results suggest new ways to couple the orientations of liquid crystals to chemical and electrical stimuli in electro-optical devices and chemical sensors.

Liquid crystalline materials are liquids with anisotropic optical and electrical properties that arise from the preferred orientations of molecules within the liquid (*1*). These materials, when placed into contact with surfaces, spontaneously assume orientations that depend sensitively on the topography and chemical functionality of the surfaces (*2*). Past studies have demonstrated that application of an electric field across a liquid crystal oriented by a surface will generally change the orientation of the bulk of the liquid crystal but not regions of the liquid crystal near the surface (so-called strong anchoring: Fig. 1A, I) (*1*, *2*). This effect forms the basis of most liquid-crystal displays (*1*). Here we report a method to chemically functionalize electrodes so as to electrically drive the orientations of liquid crystals from surfaces. By using electrodes decorated with redox-active groups that undergo reversible oxidation and reduction, surface-driven orientational transitions in liquid crystals (Fig. 1A, II) are demonstrated at voltages that are small compared with those generally required to complete a change in orientation of liquid crystal in a conventional electro-optical device (*3*). Surface-induced anchoring transitions of liquid crystals driven by chemical oxidation of patterned redox-active groups are also demonstrated (Fig. 1A, III) (*4*). These characteristics suggest that surface-driven orientational transitions using electrodes decorated with redox-active groups might find application in electronic print (*5*, *6*) or chemically responsive soft materials (*7*, *8*).

The design of the experimental system was based on three observations. First, gold electrodes functionalized with ferrocene form the basis of a structurally well-defined metal-electrolyte interface: Ferrocene undergoes a reversible one-electron oxidation to form the ferrocenium cation (Fig. 1B) (*9*, *10*). Second, studies have demonstrated that it is possible to use thermotropic liquid crystals formed from 4,4′-pentylcyanobiphenyl (5CB) and *N*-(*p*-methoxybenzylidene)-*p*-butylaniline (MBBA) as solvents for electrochemical studies of electroactive species dissolved in the bulk of liquid crystals (Fig. 1C) (*11*). Third, the ionization of acids and dissociation of surface-immobilized salts can lead to in-plane and out-of-plane orientational transitions in liquid crystals (*12*, *13*). These observations led us to hypothesize that control of the oxidation state of ferrocene on a ferrocene-decorated electrode may lead to surface-driven orientational transitions in liquid crystals.

We first investigated the influence of the oxidation state of surface-immobilized ferrocene on the orientation of either 5CB or MBBA by using benzoyl peroxide (BP, 20 mM) dissolved in the liquid crystal to oxidize the ferrocene to ferrocenium (*14*). Polycrystalline gold films were deposited so as to avoid the introduction of anisotropic topography into the structure of the gold films (*15*) and then patterned with monolayers formed from $CH_3(CH_2)_{15}SH$ and $Fc(CH_2)_{11}SH$, where Fc is ferrocene. On both the ferrocene and methyl-terminated monolayers, we measured nematic 5CB to assume an orientation that was parallel (planar) to the surface with-

Department of Chemical and Biological Engineering, University of Wisconsin–Madison, Madison, WI 53706, USA.

*To whom correspondence should be addressed. E-mail: abbott@engr.wisc.edu